Journal of Solid State Chemistry 188 (2012) 1–10

Contents lists available at SciVerse ScienceDirect

Journal of Solid State Chemistry

journal homepage: www.elsevier.com/locate/jssc

Heat capacity and neutron diffraction studies on the frustrated magnetic $Co_2(OH)(PO_4)_{1-x}(AsO_4)_x$ $[0 \le x \le 1]$ solid solution

I. de Pedro [a,b,*], J.M. Rojo [b], J. Rodríguez Fernández [a], J. Sanchez Marcos [a,1], M.T. Fernández-Díaz [c], T. Rojo [b]

[a] CITIMAC, Facultad de Ciencias, Universidad de Cantabria, 39005 Santander, Spain
[b] Departamento de Química Inorgánica, Facultad de Ciencia y Tecnología, Universidad del País Vasco, 48080 Bilbao, Spain
[c] Institut Laue-Langevin, BP 156X, F-38042 Grenoble Cedex, France

ARTICLE INFO

Article history:
Received 18 November 2011
Received in revised form
16 January 2012
Accepted 23 January 2012
Available online 31 January 2012

Keywords:
Insulation compounds
Magnetic structures
Neutron diffraction
Specific heat
Magnetostructural correlations

ABSTRACT

The $Co_2(OH)(PO_4)_{1-x}(AsO_4)_x$ $[0 \le x \le 1]$ solid solution exhibits a complex magnetic behaviour due to the bond-frustration in its magnetic structure. Heat capacity measurements of the (x=0.1–0.5) phases show a three-dimensional magnetic ordering (λ anomaly) that shifts to lower temperatures and becomes broader as the AsO_4^{3-} content increases. For x=0.75, no significant feature was observed whereas for higher arsenate ion content, x=0.9 and 1, a small maximum was detected. The magnetic structures of solid solution are consistent with the existence of predominant antiferromagnetic superexchange interactions through the |OH| and $|XO_4|$ (X=P and As) groups between the Co^{+2} ions. The substitution of PO_4^{3-} by AsO_4^{3-} anions by more than 90% substantially modifies the magnetic exchange pathways in the solid solution, leading to an incommensurate antiferromagnetic structure in $Co_2(OH)(PO_4)_{1-x}(AsO_4)_x$ [x=0.9 and 1] phases.

1. Introduction

In recent years, many hydroxyphosphate and arsenate compounds containing transition metals have been widely investigated because their complex structural chemistry offers different types of polyanionic structures, which can give rise to potential applications and interesting properties. For instance, $LiFe(OH)PO_4$ and $LiFe(OH)AsO_4$ as electrodes for lithium-ion batteries in energy storage [1,2], mixed valence arsenate with electronic conductivity [3], phosphate and arsenate with open framework structures that have versatile applications in gas separation and ion exchange [4–7], or the libethenite mineral, $Cu_2(OH)PO_4$, recently discovered, which is a good catalyst for selective oxidation of organic substrates [8–11].

The complex structural chemistry of the adamite-type M_2XO_4OH [where M= Zn, Mg, Co, Mn, Cu, etc.; X=P, As] family [12–17], with a wide variety of polymorphs [18,19], shows a large diversity of structural phases built upon $|MO_6|$ octahedra, $|MO_5|$ trigonal bypiramids linked to one another by |OH| ligands and $|XO_4|$ [X=P and As] tetrahedra [20,21]. This structural and chemical richness makes it particularly suitable for the study of the relationships between the physical properties and the crystal packing features. However, although most of these minerals have been known for many years, the study of their physico-chemical properties has been hampered due to the presence of impurities or mixed phases [12–19]. So, our interest has been focused on finding the optimized conditions to synthesize these minerals with high purity through hydrothermal synthesis. In addition, several new phases were also obtained, makinga new anddeeper study of their physico-chemical properties within this family possible [22–30].

Recently, many phosphate and arsenate compounds containing transition metals such as Co, Ni, Fe, Mn and Cu have attracted much attention in solid state physics and chemistry since the discovery of their interesting magnetic properties for insulation compounds, like magnetic frustration, field-induced magnetic transitions, incommensurate magnetic structures, etc. [22–32]. In this context, the $Co_2(OH)PO_4$ [22] phase is known as a magnetic frustrated system where an antiferromagnetic ordering and a spin-glass behaviour coexist at low temperatures. Furthermore, the partial substitution of transition metal ions in this phase shows interesting magnetic phenomena such as a spin-glass-like state in the $(Co,Ni)_2(OH)PO_4$ compounds below 10 K [26], the evolution of a three-dimensional antiferromagnetic system in the $Co_{2-x}Cu_x(OH)PO_4$ solid solution [27] to a spin-gap system in the $Cu_2(OH)PO_4$ phase [8], or stronger ferromagnetic interactions at lower temperatures in $Co_{1.7}Mn_{0.3}(OH)PO_4$ coexisting with a similar spin-glass-like state [28].

On the other hand, the total substitution of the PO_4^{3-} by AsO_4^{3-} anions in the $Co_2(OH)PO_4$ phase reveals some differences in the crystal packing features that modify the complex magnetic properties exhibited in this phase. Although $Co_2(OH)AsO_4$ is isostructural with $Co_2(OH)PO_4$ (see Fig. 1), its magnetic properties

* Corresponding author at: CITIMAC, Facultad de Ciencias, Universidad de Cantabria, 39005 Santander, Spain.
E-mail address: depedrovm@unican.es (I. de Pedro).
[1] Present address: Instituto de Ciencia de Materiales de Madrid, Consejo Superior de Investigaciones Científicas, Cantoblanco, E-28049 Madrid, Spain.

0022-4596/$ - see front matter © 2012 Elsevier Inc. All rights reserved.
doi:10.1016/j.jssc.2012.01.048

and, in particular, its magnetic structure are quite different. While the hydroxyphosphate phase exhibits a collinear magnetic structure below 71 K, hydroxyarsenate displays a sinusoidal magnetic structure with an antiferromagnetic ordering influenced by the magnetic field below 21 K [29].

The synthesis, spectroscopic properties and thermal evolution of the molar magnetic susceptibility of $Co_2(OH)(PO_4)_{1-x}(AsO_4)_x$ [$x=0$–1] solid solution have been recently published [30]. The magnetic results showed a complex behaviour in all phases with the existence of predominant three-dimensional antiferromagnetic interactions. The Neel temperature (T_N) decreased as the arsenate amount increased, going from 71 for $x=0$ to 19 K for $x=1$. At low temperatures, the magnetic signal attributed to the spin glass-like state in $Co_2(OH)PO_4$ [22,33,34] disappeared, with arsenate ion substitution, showing the presence of a ferromagnetic component, just below T_N, for the $Co_2(OH)(PO_4)_{1-x}(AsO_4)_x$ [$x=0.1$–0.75] phases. Furthemore, the disappearance of the inflexion point close to 6 K observed in the FC curve of $Co_2(OH)AsO_4$, with a slight amount of PO_4 substitution (10%), revealed changes in the magnetic ordering of the non-substituted arsenate compound [29].

Now, in order to understand these magnetic changes with anion substitution, heat capacity and neutron diffraction measurements have been carried out. In addition, the study of the magnetic exchange pathways of the solid solution with high resolution powder neutron diffraction has been performed. The analysis of these data gives us information about the changes in the magnetic frustration system of $Co_2(OH)PO_4$ that lead to a sinusoidal amplitude modulated phase in $Co_2(OH)(PO_4)_{0.1}(AsO_4)_{0.9}$ and $Co_2(OH)AsO_4$.

2. Experimental

The synthesis and physical characterisation of $Co_2(OH)(PO_4)_{1-x}(AsO_4)_x$ [$0\le x\le 1$] were previously reported [30] using hydrothermal and spectroscopic techniques. The X-ray powder diffraction data were used to evaluate the purity of the products obtained in the synthesis. The data were collected on a Philips X'Pert-MPD diffractometer in Bragg-Brentano geometry operating at 40 kV and 30 mA, with Cu $K_{\alpha 1}$ radiation ($\lambda\approx 1.5406$ Å) and steps of 0.02° in a fixed time counting of 6 s from 10° to 90°. The patterns were fitted using the pattern matching routine of the program FULLPROF [35] in orthorhombic cells with the Pnnm space group, starting from single crystal data by Harrison et al. [36] and Séller et al. [37] for the $Co_2(OH)PO_4$ and $Co_2(OH)AsO_4$ phases, respectively.

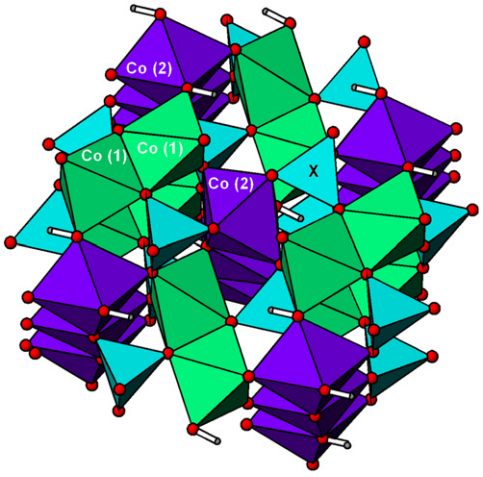

Fig. 1. Schematic drawing of the $Co_2(OH)XO_4$ (X=P, As) crystal structure view along the c direction. Green and purple polyhedra are occupied by the Co(1) and Co(2) ions, respectively, and the XO_4 groups are represented by blue tetrahedra. Open circles correspond to the oxygen atoms, and little circles show the hydrogen atoms.

Powder neutron diffraction measurements were performed on the D1B and D2B powder diffractometers, at the Institute Laue-Langevin of Grenoble, using wavelengths of 2.525 and 1.5938 Å, respectively. About 5 g of $Co_2(OH)(PO_4)_{1-x}(AsO_4)_x$ [$0\le x\le 1$] phases were employed in the neutron diffraction experiments, placed in a cylindrical vanadium container and held in a liquid helium cryostat. The high resolution of D2B was used to obtain extensive and accurate structural and magnetic data at room temperature and 2 K, respectively, over a large angular range $0\le 2\theta\le 150$. High flux and medium resolution of D1B at 2.525 Å were used to study the thermal evolution of the magnetic and crystalline structures in the temperature range 1.8–90 K. The diffraction patterns were collected every 2 K and 25 min in the angular range $10\le 2\theta\le 90$. The Rietveld method [38] was used to refine the nuclear and magnetic structures. All the patterns were analyzed using the FULLPROF program suite [35]. The background was fitted using a polynomial refinable function, and the D1B patterns were refined sequentially, taking as the starting parameters for each pattern those resulting from the refinement of the preceding one. A pseudo-Voigt function was chosen to generate the line shape of the diffraction peaks.

Heat capacity measurements were carried out with a standard QD PPMS device by a traditional relaxation method using a two-tau model. The samples were obtained by compressing the original polycrystalline powder and the weight ranged from 7.3 to 11.2 mg. In order to assure good thermal contact, the sample was glued to the sample-holder using Apiezon N grease. Data were collected with zero field and under an applied field of 90 kOe from 1.8 to 300 K. The addenda (sample-holder plus grease) was measured at different magnetic fields prior to the sample measurements and then subtracted from the total heat capacity in order to get the sample heat capacity.

3. Results and discussions

3.1. Specific heat measurements

The temperature dependence of the molar heat capacity (Cp) for the $Co_2(OH)(PO_4)_{1-x}(AsO_4)_x$ [$0\le x\le 1$] solid solution between 1.8 and 150 K in the absence of an external magnetic field is shown in Fig. 2. The main feature in calorimetric measurements is attributed to a three-dimensional magnetic ordering peak (λ anomaly) observed in $Co_2(OH)PO_4$, which shifts to lower temperatures (from 69.7 K for $x=0$ to 64.1, 56.2 and 44.1 for $x=0.1$, 0.25 and 0.5, respectively) and becomes broader as the AsO_4^{3-} content increases. For $x=0.75$ no significant feature appears in the whole temperature range studied, whereas for higher AsO_4^{3-} content, a small peak ($\Delta Cp=1$ and 2 J/Kmol for $x=0.9$ and 1) centred at 20.2 and 18.6 K, respectively, is observed (see Table 1). Although the small peak does not posses the typical characteristics of a second order transition (λ anomaly) it can be associated with the establishment of a three-dimensional antiferromagnetic ordering in good agreement with the magnetic susceptibility data [30]. We also measured the heat capacity under an applied magnetic field of $B=9$ T (not shown). For the $Co_2(OH)(PO_4)_{1-x}(AsO_4)_x$ [$x=0.1$–0.9] compounds the effect of the magnetic field is very small, reflecting the existence of strong anisotropy. However, the heat capacity measurements of the $Co_2(OH)AsO_4$ phase presented an unexpected behaviour with the applied magnetic field (the maximum associated to the three-dimensional ordering grows with field and becomes better defined) that suggest the existence of a weak magnetocrystalline anisotropy. This effect is attributed to a change in the type of magnetic structure from incommensurate to commensurate via the effect of the

magnetic field [29]. The Cp difference between 0 and 9 T [Cp(0 T)–Cp(9 T)] for the $x=0.75$ compound is plotted in the upper inset of Fig. 2 showing a broad peak centred at 34 K. Although the maximum difference is 0.6 J/Kmol, it represents 4% of the total Cp at 34 K, indicating a magnetic contribution in the $Co_2(OH)(PO_4)_{0.25}(AsO_4)_{0.75}$ phase in good agreement with the magnetic susceptibility [30] and neutron diffraction data.

On the other hand, no anomalies were observed below the three-dimensional magnetic ordering in any of the phases (see lower inset of Fig. 2), which prompted us to propose that the other magnetic contributions detected in the magnetic susceptibility measurements (ferromagnetic components) are not of a long-range type. Finally, above the magnetic transition, the molar heat capacity (Cp) increased continuously due to the phonon contribution and showed no tendency towards saturation even up to room temperature, where the value of Cp ranged from 153 to 164 J/Kmol (see Table 1). This behaviour is due to the presence of light atoms (O and H) with very high excitation energy, which causes that the theoretical Dulong and Petit value (near to 225 J/Kmol) [39] to be reached above room temperature, in good agreement with other arsenates and phosphates of the adamite-type family [22–30].

The phonon heat capacity was determined by fitting the high temperature part of Cp ($T>80$ K) to a Debye model [40] and considering two different phonon spectra, (heavy atoms, n_1, with a Debye temperature θ_1 and light atoms, n_2, with a Debye temperature θ_2), as was successfully used for $Co_2(OH)PO_4$ and $Co_2(OH)AsO_4$ [22,29]. The main obtained parameters are given in Table 1. The estimated Debye temperatures range from 263 to 274 K and from 1000 to 1086 K for θ_1 and θ_2, respectively. The magnetic contribution to the heat capacity (C_{mag}) in each solid solution was obtained by subtracting the corresponding phonon contribution (C_{pho}), see Fig. 3. At first glance, what can be seen is that the two ends of the family ($x=0$ and $x=1$) exhibit different behaviours. These behaviours evolve continuously, converging in a broad maximum for $x=0.75$. Starting with the pure arsenate phase, C_{mag} exhibits a small peak superimposed on a broad maximum. One of the most plausible explanations for this behaviour is the contribution to the magnetic heat capacity of chains and dimmers in the form of a two-dimensional magnetic order, as a precursor of the three-dimensional ordering [29]. This was analyzed with a quasi-two-dimensional antiferromagnetic Heisenberg model [41]. The comparison of the magnetic heat capacity data with this theoretical model showed that the dimensionless interplane coupling $\alpha=J_\perp/J$, where $J(J_\perp)$ is the strength of the intra-planar (inter-planar) coupling, is $\alpha<1$. As can be observed in Fig. 3, the introduction of phosphate into the pure arsenate phase favours the two-dimensional order, decreasing the α value, $Co_2(OH)(PO_4)_{25}(AsO_4)_{75}$ being the phase with the lowest one. For higher phosphate content, the broad maximum shifts to higher temperatures and evolves into a better defined peak; i.e., for $x<0.75$, the introduction of phosphate favours the three-dimensional character of the magnetic structure. The magnetic entropy, $Sm=\int=C_{mag}/T)\ dT$ (not shown),

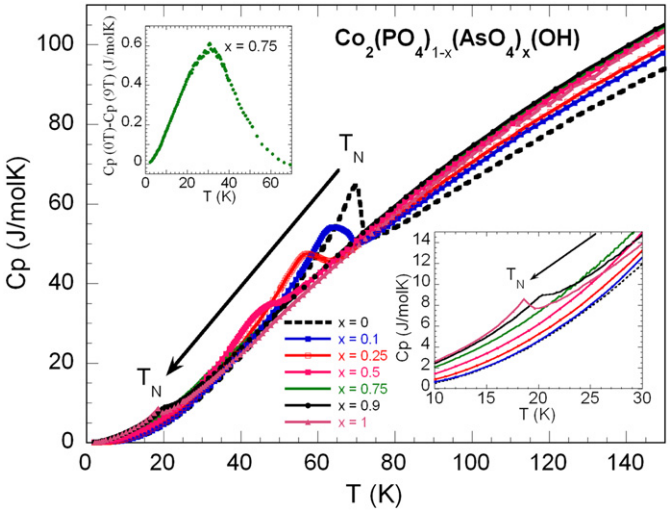

Fig. 2. Specific heat of $Co_2(OH)(PO_4)_{1-x}(AsO_4)_x$ [$0\le x\le 1$] between 1.8 and 150 K. Upper inset shows the specific heat difference of $Co_2(OH)(PO_4)_{0.25}(AsO_4)_{0.75}$ between 0 and 9 T. Lower inset displays an enlargement of low temperature data.

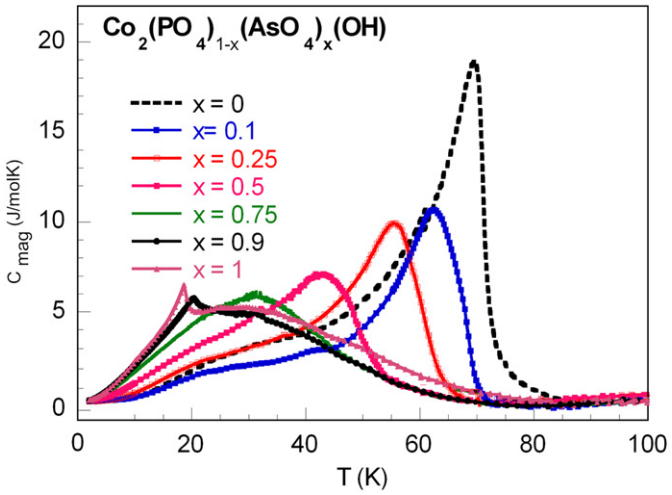

Fig. 3. Magnetic contribution of Cp (C_{mag}) calculated by subtracting the phonon contribution (C_{pho}) for $Co_2(OH)(PO_4)_{1-x}(AsO_4)_x$ [$0\le x\le 1$].

Table 1
Summary of specific-heat data of the $Co_2(OH)(PO_4)_{1-x}(AsO_4)_x$ ($x=0$–1) compounds.

$Co_2(OH)(PO_4)_{1-x}(AsO_4)_x$	$x=0$	$x=0.1$	$x=0.25$	$x=0.5$	$x=0.75$	$x=9$	$x=1$
T_{max} (K)	69.7	64.1	56.2	44.1		20.2	18.6
Inflexion point (K)	71.3	65.2	56.9	45.5		21.4	20.2
Cp_at 300 K (J/K mol)	153	162	159	154	162	164	160
C_{mag}_at T_{max} (J/K mol)	18.6	11.2	10.6	7.4	6.2	6.1	6.8
Debye model(#)							
Range of fit (K)	>80	>80	>80	>80	>80	>80	>80
n_1	3.2	3.2	3.3	3.4	3.5	3.6	3.6
n_2	5.8	5.8	5.7	5.6	5.5	5.4	5.4
θ_1 (K)	263	270	274	267	265	269	270
θ_2 (K)	1086	1074	1066	1020	1015	1000	1048

(#) The high temperature data fitted by a Debye model considering the existence of two-phonon spectra. The unit cell contains three heavy atoms (n_1) with a Debye temperature θ_1 and six light atoms (n_2) with a Debye temperature θ_2.

tends to saturate well above the magnetic transition, at around 80 K, in all compounds. The values range from 5.5 to 9.3 J/mol K for $x=0.1$ and $x=1$, respectively. For all phases, the magnetic entropy is lower than the theoretical value $S_{mag}=2R\ln(2S+1)$, with $S=3/2$ for Co^{2+}. The most plausible explanation for this entropy reduction is the existence of remanent entropy below 2 K, associated to the different degrees of frustration of the magnetic structures. Another additional explanation, connected with the previous one, is the existence of a small percentage of magnetic ions, which do not contribute to the magnetic order.

3.2. Powder neutron diffraction

3.2.1. Nuclear structure

The structural refinements of the solid solution were carried out from high resolution powder neutron diffraction patterns (D2B) recorded at room temperature with $\lambda=1.5938$ Å. In the case of the $Co_2(OH)(PO_4)_{0.5}(AsO_4)_{0.5}$ phase, only D1B neutron diffraction data recorded with $\lambda=2.522$ Å at 100 K were available. The diffraction patterns were fitted using the Pnnm space group and, as a starting point, we took the cell parameters reported for X-ray diffraction [30]. The room temperature structural parameters and the reliability factors are summarized in Table 2. It is noteworthy that the quality of the results allows us both to localise the hydrogen ions in the structure and to determine the As/P ratio, this latter showing good agreement with the elemental analysis data. Details of the final refined positional and thermal parameters obtained of high resolution neutron diffraction data are included as electronic supplementary information (ESI) (CIF files).

Taking into account the structural data obtained from the high resolution diffraction patterns (D2B) at room temperature, reasonable Rietveld refinements of the D1B diffraction patterns at 100 K were obtained in these compounds. The data obtained from the Rietveld fits are quite similar to those of the room temperature structure but show small differences associated to thermal effect. Thus, the cell parameters obtained from powder neutron diffraction (D2B and D1B) at 300 and 100 K exhibit a linear variation with the phosphate substitution degree, x (see Table 2). Lattice parameters and cell volume increase with the gradual substitution of phosphate by arsenate ions following Vegard's law in the whole range of composition, in good agreement with both the periodic trend in radius of Group 15 of the periodic table and the results obtained from X-ray diffraction [30].

The crystal structure of the solid solution consists of a condensed network of vertex and edge-sharing CoO_6, CoO_5 yXO_4 (X=P and As) subunits (see Fig. 1). The Co ions are disposed in two different crystallographic positions. On one hand, the Co(1) is fivefold coordinated by O(1), O(3) and O(4)H oxygen atoms in approximately trigonal bipyramidal geometry. The equatorial Co(1)–O(1)ii and Co(1)–O(3) bond distances range from 2.091(1) to 2.004(1) Å and from 2.011(9) to 2.003(4) Å, respectively, whereas the apical Co(1)–O(1)iii and Co(1)–O(4)H bond distances range from 1.996(8) to 1.959(9) Å and 2.079(9) to 1.968(9) Å, respectively. (Symmetry code: ii=$1/2-x$, $1/2+y$, $1/2-z$; iii=$x-1/2$, $1/2-y$, $z-1/2$). On the other hand, the Co(2) atoms exhibit a distorted octahedral geometry, coordinated by O(2), O(3) and O(4)H oxygen atoms, with two long apical bond distances, Co(2)–O(3) from 2.263(3) to 2.224(7) Å, and four shorter equatorial links, Co(2)–O(2) from 2.084(4) to 2.050(9) Å and Co(2)–O(4)H from 2.116(7) to 2.007(9) Å in the *cis* configuration. The octahedra share the O(2)–O(2) and the O(4)H–O(4)H edges, giving rise to linear chains propagated along the z-axis (Fig. 1). The trigonal bipyramids constitute dimeric entities, sharing the O(1)–O(1) edge. The axial and equatorial O–Co(2)–O mean angles in the CoO_6 octahedra are around 170° and 92°, respectively. For the CoO_5 polyhedra, each trigonal bipyramid exhibits three sets of O–Co(1)–O angles around 91°, 122° and an axial one of 168°. Both sublattices, Co(2) chains and Co(1) dimers are cross-linked via oxygen [O(3), O(4)H] bridges.

The phosphate–arsenate groups exhibit three different bond lengths where the mean distances increase with the gradual substitution of phosphate by arsenate ions from 1.57(1) to 1.69(1) Å. It is noteworthy that these bond lengths in each compound are fairly regular as in the majority of the adamite-type M_2XO_4OH [where M=Zn, Mg, Co, Mn, Cu, etc.; X=P, As] compounds [12–19]. These facts affect the magnetic properties of these geometrically frustrated cobalt phosphate–arsenate compounds, as will be analyzed later in the magnetostructural correlations. Finally, the chain of octahedra, the dimeric units, and the phosphate–arsenate anions share corners, resulting in a condensed three-dimensional structure without any identifiable channels or pores.

Table 2
Details of Rietveld refinements from neutron diffraction patterns (D2B) at room temperature for $Co_2(OH)(PO_4)_{1-x}(AsO_4)_x$ ($x=0.1$, 0.25, 0.75 and 0.9) and (D1B) at 100 K for $Co_2(OH)(PO_4)_{0.5}(AsO_4)_{0.5}$.

Compound	$x=0.1$	$x=0.25$	$x=0.5$	$x=0.75$	$x=0.9$
Space group	*Pnnm* (No. 58)	*Pnnm* (No. 58)	*Pnnm* (No. 58)	*Pnnm* (No. 58)	*Pnnm* (No. 58)
a (Å)	8.0508(2)	8.0979(3)	8.119 (1)	8.2118(4)	8.2446(1)
b (Å)	8.3945(2)	8.4324(4)	8.464 (1)	8.5340(5)	8.5666(1)
c (Å)	5.9532(2)	5.9661(3)	5.972 (1)	6.0123(3)	6.0313(1)
V (Å^3)	402.34(2)	407.40(2)	410.1 (1)	421.34(4)	425.98(1)
Instrument	D2B (ILL)	D2B (ILL)	D1B (ILL)	D2B (ILL)	D2B (ILL)
T (K)	300	300	100	300	300
Wavelength (Å)	1.5938	1.5938	2.522	1.5938	1.5938
Monochromator	Ge (335)	Ge (335)	Ge (311)	Ge (335)	Ge (335)
Z	4	4	4	4	4
2θ range (°)	10–150	10–150	10–90	10–150	10–150
2θ step-scan increment (°)	0.05	0.05	0.2	0.05	0.05
No. of reflections	365	372	96450	384	376
No. of profile parameters	36	36	26	36	36
Reliability factor (%)					
$R_p=\Sigma\lvert y_{i,\,obs}-(1/c)y_{i\,calc}\rvert/\Sigma y_{i,\,obs}$	17.0	15.2	15.3	13.1	12.6
$Rw_p=[\Sigma w_i\lvert y_{i,\,obs}-(1/c)y_{i,\,calc}\rvert^2/\Sigma w_i\,[y_{i,\,obs}]^2]^{1/2}$	15.1	13.7	11.6	11.6	11.1
$R_B=[\Sigma\lvert I_{obs}-I_{calc}\rvert/\Sigma I_{obs}$	7.79	6.82	3.91	4.62	6.31
χ^2	1.297	1.232	3.53	1.176	1.333

D2B powder neutron diffraction unit-cell parameters from $Co_2(OH)PO_4$[22]: $a=8.040(1)$ Å, $b=8.376(1)$ Å, $c=5.951(1)$ Å and $V=399.8(1)$ Å^3 and $Co_2(OH)AsO_4$[29]: $a=8.2587(2)$ Å, $b=8.5801(1)$ Å, $c=6.0391(1)$ Å and $V=427.94(3)$ Å^3.

3.2.2. Magnetic structure

Powder neutron diffraction patterns at 2 K for the solid solution were collected in the D2B and D1B powder diffractometers. The D1B neutron diffraction patterns for $Co_2(OH)(PO_4)_{1-x}(AsO_4)_x$ (x=0.25, 0.5, 0.75, 0.9 and 1) between 5° and 85° (2θ) are represented in Fig. 4. The experimental, calculated and difference diffraction profiles of $Co_2(OH)(PO_4)_{1-x}(AsO_4)_x$ (x=0.1 and 0.9) in D2B, as representative, are shown in Fig. 5. All the patterns exhibit extra magnetic peaks, indicating that all the compounds have a long range magnetic ordering at low temperatures. The different positions of the magnetic peaks (Fig. 4) when the percentage of arsenate substitution is higher than 75%, reveal significant changes in the magnetic structure. For the $Co_2(OH)(PO_4)_{1-x}(AsO_4)_x$ (x=0.1–0.75) phases, all magnetic peaks were indexed with a propagation vector k=(0, 0, 0) referenced to the room temperature unit cell indicating that both the magnetic and nuclear unit cells were similar. As was observed in $Co_2(OH)PO_4$ [22], a very intense (0 1 0) reflection at $2\theta \approx 12°$ appeared, arising from long range antiferromagnetic ordering in these samples. It is worth mentioning that the intensity of this reflexion decreases as arsenate substitution increases (Fig. 4). This result is associated with an increasing of the frustration in the magnetic structure due to a higher disorder of the magnetic sites [Co(2) octahedral chains and Co(1) trigonal bipyramidal dimers] in good agreement with the magnetic heat capacity data. For the $x > 0.75$ compounds, all the magnetic peaks were indexed with a propagation vector k=(0, δ, 0). In the case of the $Co_2(OH)(PO_4)_{0.1}(AsO_4)_{0.9}$ phase the magnetic peaks were indexed with the propagation vector k=(0, 0.32, 0) at the lowest temperature (2 K), indicating that the magnetic unit cell is almost three times larger than nuclear unit cells. Finally, for the non-substituted arsenate compound, the propagation vector, k, evolves to (0, 0.43, 0) at 2 K, showing the existence of an incommensurate antiferromagnetic structure along the b direction.

Following the symmetry-representation analysis [42] using the program BASIREPS [43], and taking into account the magnetic structure of the $Co_2(OH)XO_4$ (X=P and As) compounds [22,29], a

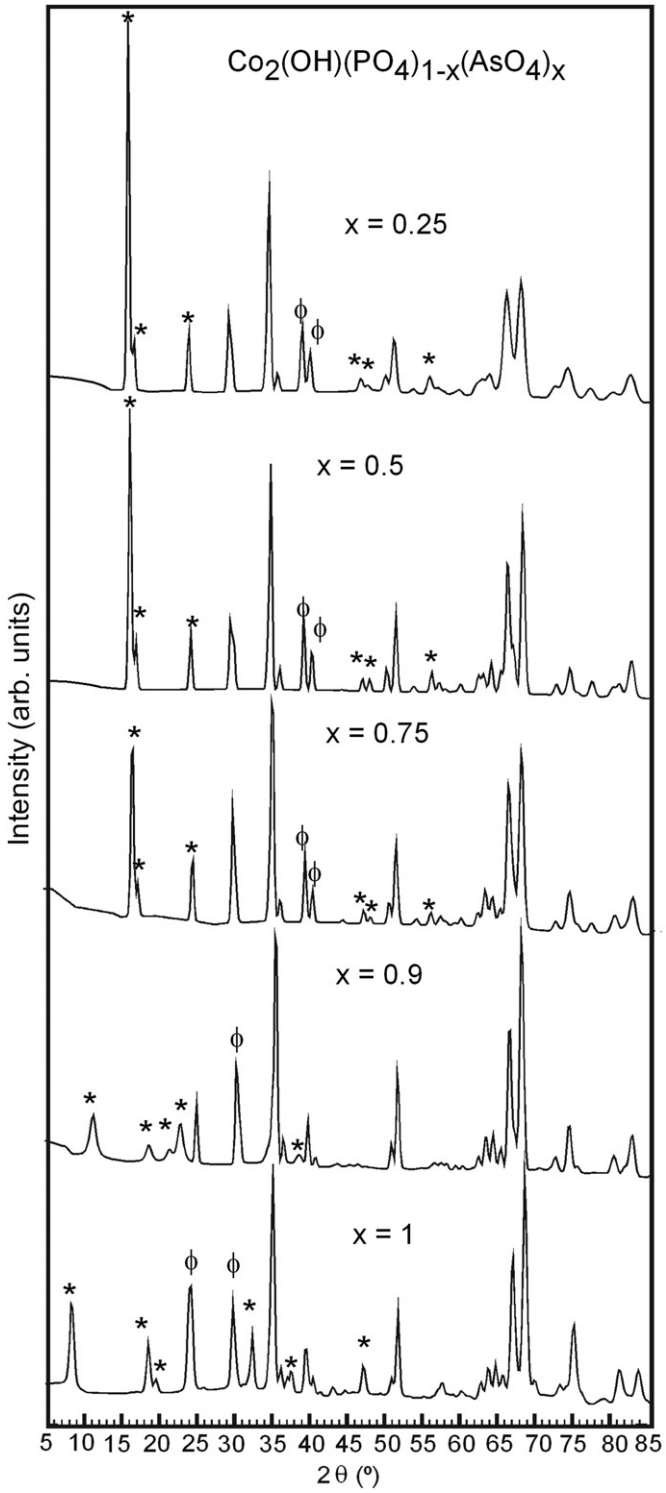

Fig. 4. Low temperature (2 K) D1B neutron diffraction data for $Co_2(OH)(PO_4)_{1-x}(AsO_4)_x$ (x=0.25, 0.5, 0.75, 0.9 and 1) showing the change of intensity and the shift of the magnetic peaks (*) and magnetic/structural contributions (ϕ) with the arsenate content.

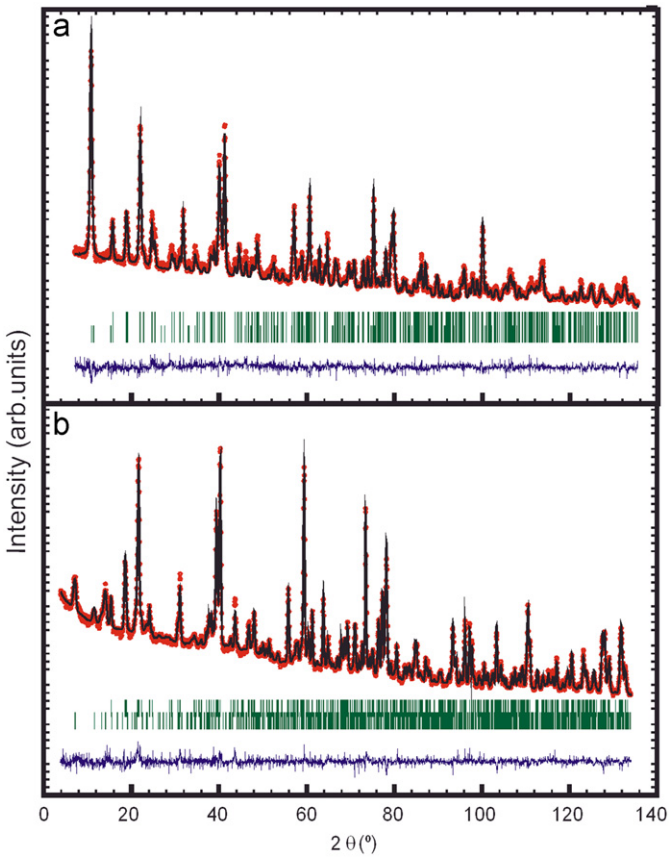

Fig. 5. D2B neutron diffraction data of (a) $Co_2(OH)(PO_4)_{0.9}(AsO_4)_{0.1}$ and (b) $Co_2(OH)(PO_4)_{0.1}(AsO_4)_{0.9}$ (λ=1.5938 Å) at 2 K. Positions of the Bragg reflections for the nuclear (first row) and magnetic (second row) structures are presented. The difference curves are plotted at the bottom.

best fit of the D2B and D1B experimental patterns for phosphate–arsenate phases at 2 K has been obtained (see supplementary material for Figs. S1 and S2). In all compounds, the refinement of the components from the magnetic moments gives $Mx=0$ and $My=0$, indicating that they lie in the c direction. The magnetic discrepancy factors are $R_{mag}=15.3$, 7.63, 10.2 and 14.3 for $x=0.1$, 0.25, 0.75, 0.9 from D2B data and $R_{mag}=9.70$, 8.53, 5.35 and 9.60 for $x=0.25$, 0.5, 0.75, 0.9 from D1B data, respectively. The components of the refined magnetic moments of Co(1) and Co(2) range from 3.53(1) to 1.43(1) μ_B and from 3.84(1) to 2.47(2) μ_B, respectively, with a resultant magnetic moment of 3.68(2), 3.12(1), 2.55(1), 2.23(1), 1.95(2), 3.11(1) and 3.22(2) μ_B for $x=0$, 0.1, 0.25, 0.5, 0.75, 0.9 and 1, respectively per Co^{2+} ion.

The ordering of the magnetic moments from the two sublattices in three unit cells, compatible with the symmetry operations, is shown in Fig. 6. As can be seen, the magnetic framework of all phases reveals the existence of ferromagnetic couplings along the c-axis in the trigonal bipyramidal dimers [sublattice of Co(1)] and octahedral chains [sublattice of Co(2)]. The three-dimensional (3D) antiferromagnetic ordering is formed by ferromagnetic layers in the xz plane that are in an antiparallel disposition, stabilizing the overall antiferromagnetic arrangement through the $|OH|$ and $|XO_4|$ (X=P and As) groups. However, in the case of the $Co_2(OH)(PO_4)_{1-x}(AsO_4)_x$ ($x=0.9$ and 1) compounds they are modulated in the b direction (see the wavy arrow in Fig. 6). In this way, the Co^{2+} moments are ordered with the magnetic moment modulated in a longitudinal sinusoidal wave perpendicular to the propagation vector where the magnetic cell parameter along b direction is higher than that of the unit cell.

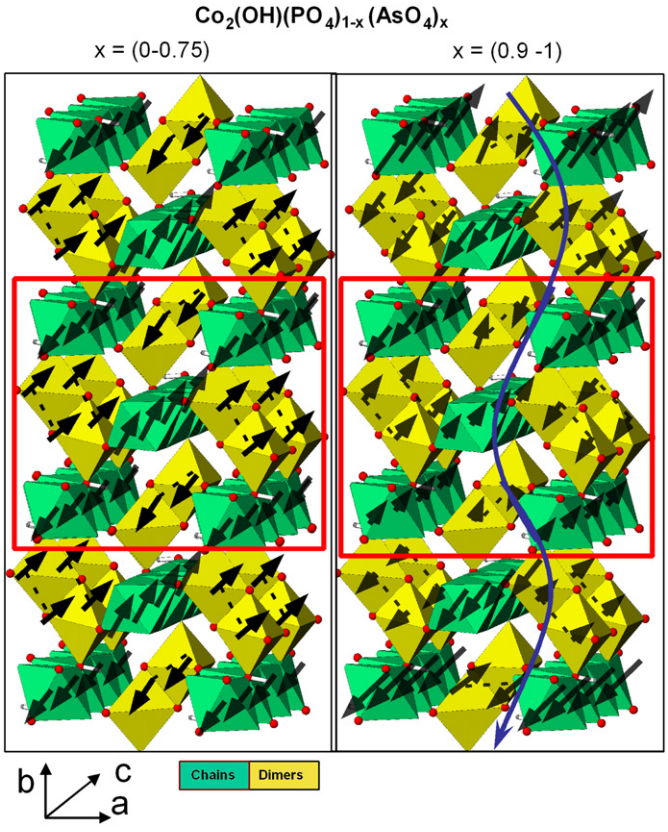

Fig. 6. Magnetic structures of $Co_2(OH)(PO_4)_{1-x}(AsO_4)_x$ [$0 \le x \le 1$]. The ordering of the magnetic moments of Co^{2+} is in c direction for the two crystallographic positions (dimers and chains) in all compounds. The unit cell is surrounded by a red line. Note that for the incommensurate antiferromagnetic structure of $Co_2(OH)(PO_4)_{1-x}(AsO_4)_x$ [0.9 and 1], the sinusoidal modulation of the magnetic moments is also shown (blue). The phosphate–arsenate groups have been omitted for greater picture clarity. (For interpretation of the references to color in this figure legend, the reader is referred to the web version of this article.)

The thermal evolution of the neutron diffraction patterns for $Co_2(OH)(PO_4)_{1-x}(AsO_4)_x$ ($x=0.25$, 0.5, 0.75, 0.9 and 1) from 1.8 to 80 K was followed in the D1B instrument. The temperature dependence for $Co_2(OH)(PO_4)_{1-x}(AsO_4)_x$ ($x=0.25$ and 0.9), as representative, is shown in Fig. 7(a). The rest of the phases show similar thermal behaviour. All curves exhibit extra magnetic peaks generated by the antiferromagnetic long range ordering at temperatures around 61, 50, 40, 23 and 22 K for $x=0.25$, 0.5, 0.75, 0.9 and 1. These ordering temperatures should be considered as approximate, taking into account that the magnetic susceptibility and heat capacity measurements are the best assessments to obtain the Néel temperature (Table 1). It is noteworthy that the intensity of the magnetic reflections in all phases increases monotonically below T_N and reaches saturation at low temperature. The existence of anomalies indicating a modification of the long-range spin arrangement was not observed.

The magnetic moment was refined from the D1B data at all available temperatures. The thermal dependence of the ordered magnetic moments for $Co_2(OH)(PO_4)_{1-x}(AsO_4)_x$ ($x=0.25$ and 0.9), as representative, is shown in Fig. 7(b). The rest of the phases show similar behaviour with the temperature. The occupation and thermal factor were taken from the analysis of the D2B data at 2 K. As can be seen, the curves and the ordering temperature for both sublattices [Co(2) octahedral chains and Co(1) trigonal bipyramidal dimers] are similar. The magnetic moments of both sublattices rapidly increase from a temperature lower than T_N with a change in the slope at around 40, 25, 18, 8 and 12 K for $x=$(0.25, 0.5, 0.75, 0.9 and 1), respectively. From these temperatures, the magnetic moments slowly increase with practically linear variation reaching a saturation value at 2 K. It is to be noted that the refined magnetic moments of the Co(2) are always higher than those of the Co(1) in all of the temperature and composition ranges studied. This behaviour was also observed in the $(Co,M)_2(OH)PO_4$ (M=Cu and Ni) phases [26,27] and was attributed to the distinct crystal effects on both sublattices [29,44]. Moreover, in this solid solution, it could be due to higher frustration in the Co(1) sublattice. In addition, the δ-component of the magnetic propagation vector k of $Co_2(OH)(PO_4)_{0.1}(AsO_4)_{0.9}$ decreases with increasing temperature [see inset of Fig. 7(b)]. This reduction is less than that of the non-substituted arsenate phase ($\Delta\delta=0.015$ and 0.10 for $x=0.9$ and 1, respectively), indicating the existence of a stronger magnetocrystalline anisotropy than that of the non-substituted phase in good agreement with the heat capacity data with magnetic field applied.

The evolution of the magnetic moments (Mz) of both sublattices [Co(1) dimer and Co(2) chain] at 2 K with arsenate substitution is given in Fig. 8. In the case of the $Co_2(OH)(PO_4)_{1-x}(AsO_4)_x$ ($x=0$–0.75) compounds, with commensurate antiferromagnetic structure, the magnetic moments of both sublattices exhibit a roughly linear decrease of the values with the gradual substitution of phosphate by arsenate ions from 3.53(1) and 3.84(1) μ_B to 1.43(1) and 2.47(2) μ_B for dimers and chains, respectively. However, for higher substitutions ($x \ge 0.9$), the value of the magnetic moments rapidly increases to 2.90(2) and 3.32(1) μ_B for the Co(1) and Co(2) ions, respectively. This evolution is associated with both an increasing of the magnetic frustration and the transition of the magnetic structure from collinear AF to incommensurate AF magnetic structure in the solid solution by the effect of the insertion of a higher anion in the $Co_2(OH)PO_4$ phase (for $x > 0.75$). This last fact will be explained later by following the change of the magnetic exchange pathways.

3.3. Magnetostructural correlations

The transition from collinear AF to incommensurate AF magnetic structure in the solid solution must be based on the different

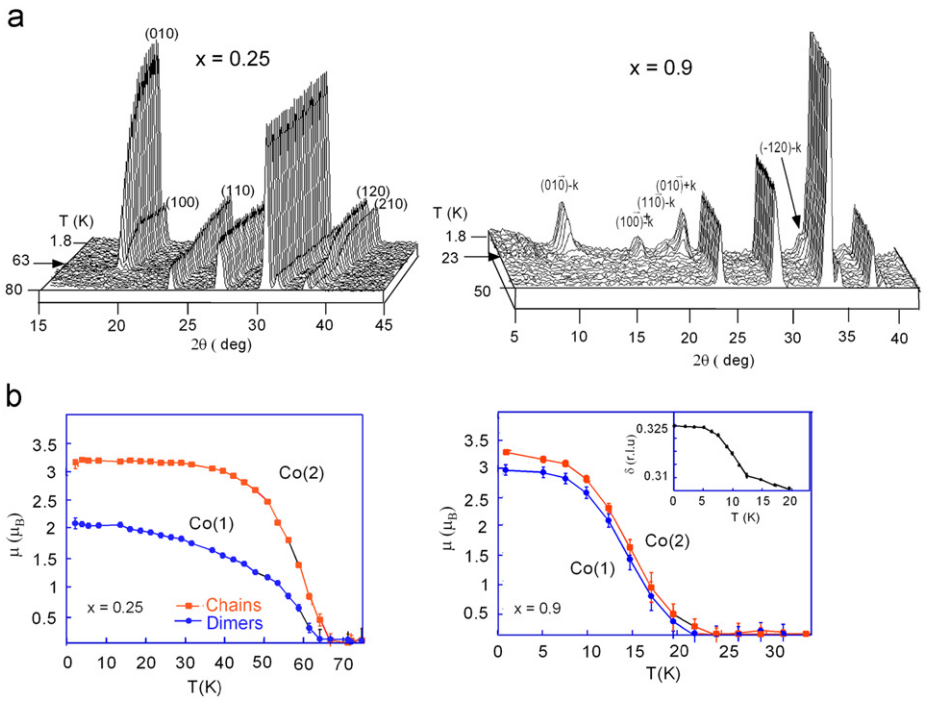

Fig. 7. (a) Thermal evolution of the D1B patterns of $Co_2(OH)(PO_4)_{0.75}(AsO_4)_{0.25}$ and $Co_2(OH)(PO_4)_{0.1}(AsO_4)_{0.9}$ between 2 and 80 K. (b) Magnetic moment for $Co_2(OH)(PO_4)_{0.75}(AsO_4)_{0.25}$ and $Co_2(OH)(PO_4)_{0.1}(AsO_4)_{0.9}$ refined from neutron data obtained with D1B as a function of temperature for chains and dimers of the Co^{2+} ions. The inset shows the magnitude of the propagation vector $(0, \delta, 0)$ of $Co_2(OH)(PO_4)_{0.1}(AsO_4)_{0.9}$ as a function of temperature. Solid lines are only visual guidelines.

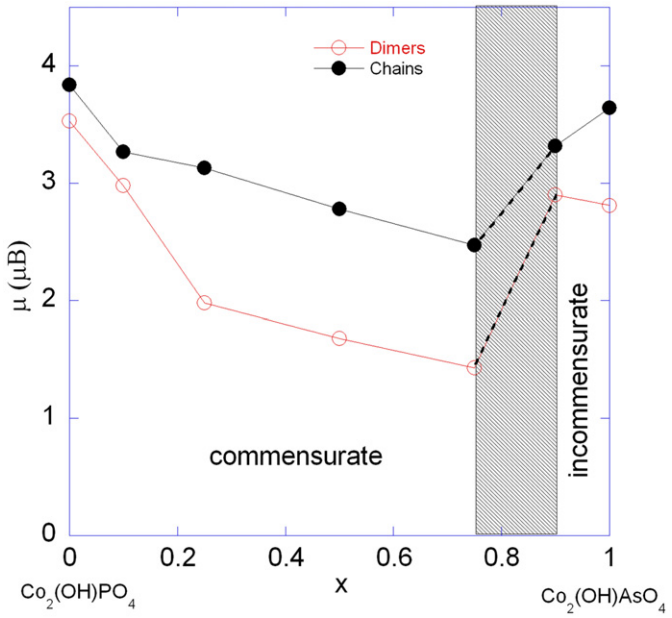

Fig. 8. Magnitude of the magnetic moments of chains and dimers at 2 K obtained in D2B (x=0, 0.1, 0.25, 0.75, 0.9 and 1) and D1B (x=0.5) in $Co_2(OH)(PO_4)_{1-x}(AsO_4)_x$ $[0 \le x \le 1]$. Solid lines are visual guidelines. The thin broken curve marks a boundary that is unresolved in the powder neutron diffraction pattern.

exchange magnetic pathways when the substitution of PO_4^{3-} for AsO_4^{3-} anions is higher than 75%. If we consider the structural features of the $Co_2(OH)(PO_4)_{1-x}(AsO_4)_x$ $[0 \le x \le 1]$ solid solution, we can deduce that direct Co–Co interactions are not present in these compounds. The shorter Co–Co distances through the space range between 2.80 and 3.70 Å, the superexchange interactions being responsible for the magnetic ordering in this system Table 3. The main interatomic distances and angles obtained from high resolution neutron diffraction data are included as electronic supplementary information (ESI) (CIF. files).

The superexchange interactions are well understood for a simple cation-anion-cation pathway with interactions that are strongly antiferromagnetic for a linear 180° Co–O–Co bond angle, and ferromagnetic for an orthogonal angle of 90°, with the crossover at around 106° [45,46]. For the $Co_2(OH)(PO_4)_{1-x}(AsO_4)_x$ $[0 \le x \le 1]$ solid solution the main interactions are present as [47,48] (i) superexchange intradimer interactions via oxygen involving metal $d_{x^2-y^2}$ orbitals in both the edge-sharing $[Co(1)_2O_6(OH)_2]$ trigonal bipyramidal dimers and $[Co(2)O_4(OH)_2]$ octahedral chains whose angles range from 89.0° to 103.0° leading to ferromagnetic interactions (see Fig. 6 and Table 3). (ii) superexchange interactions Co(1)–O(4)H–Co(2) with a mean exchange angle of 124° giving rise to antiferromagnetic couplings across the b direction. (iii) magnetic exchange pathway, Co(1)–O(3)–Co(2), between dimers and their neighbour chains. It is worth mentioning that this last magnetic interaction shows a change in the magnetic coupling due to the variation of the bond angle (see Table 3, Figs. 6 and 9). In this way, in the non-substituted hydroxyphosphate, this magnetic exchange exhibits an angle of 107° (with ferromagnetic interactions through the xz plane), which is considered essential in the competition between dimers and chains in this magnetic frustration system [22]. As obtained from high resolution powder neutron diffraction data, the Co(1)–O(3)–Co(2) magnetic exchange pathway angle increases from 107° to 112.5° (see Table 3) also showing ferromagnetic interactions in the collinear AF structure of the $Co_2(OH)(PO_4)_{1-x}(AsO_4)_x$ $[x \le 0.75]$ phases. For higher anion substitution (x=0.9), the value of this superexchange angle rises to 114.1°, showing a change in the magnetic coupling (from F to AF), resulting in a global antiferromagnetic structure modulated in amplitude with a propagator vector k=(0, 0.32, 0) (almost three times bigger than that of the nuclear unit cell). Moreover, for the non-substituted arsenate compound, the magnetic exchange Co(1)–O(3)–Co(2) evolves to 116.9°, modifying the propagation

Table 3
Selected angles (°) related to the possible magnetic superexchange pathways for $Co_2(OH)XO_4$ (X=P and As).

	Length of exchange pathway Angles (°)											
	Co–O–Co						**O–X–O**					
	***x*=0**	***x*=0.1**	***x*=0.25**	***x*=0.75**	***x*=0.9**	***x*=1**	***x*=0**	***x*=0.1**	***x*=0.25**	***x*=0.75**	***x*=0.9**	***x*=1**
Co(1)–O(1)–Co(1)	101.6	102.7	102.6	102.4	102.7	103.0						
Co(1)–O(1)–X-O(3)–Co(1)							110.2	110.7	109.0	109.1	110.3	110.2
Co(1)–O(4)H–Co(2)	123.2	123.8	122.6	124.2	124.8	126.2						
Co(1)–O(3)–Co(2)	**107.0**	**109.3**	**109.8**	**112.5**	**114.1**	**116.9**						
Co(1)–O(3)–X–O(2)–Co(2)							110.2	110.5	109.4	112.9	110.4	112.0
Co(2)–O(4)H–Co(2)	92.4	90.7	91.1	94.0	89.0	91.7						
Co(2)–O(2)–Co(2)	92.1	94.2	94.1	93.5	95.9	97.2						
Co(2)–O(2)–X–O(3)–Co(2)							110.2	110.5	11.5	112.9	110.4	112.0
	Co–O–X						**X–O–Co**					
	***x*=0**	***x*=0.1**	***x*=0.25**	***x*=0.75**	***x*=0.9**	***x*=1**	***x*=0**	***x*=0.1**	***x*=0.25**	***x*=0.75**	***x*=0.9**	***x*=1**
Co(1)–O(1)–Co(1)												
Co(1)–O(1)–X–O(3)–Co(1)	133.0	130.0	133.3	126.9	127.1	125.6	131.0	133.4	133.7	128.7	133.5	126.07
Co(1)–O(4)H–Co(2)												
Co(1)–O(3)–Co(2)												
Co(1)–O(3)–X–O(2)–Co(2)	125.0	133.4	133.7	128.7	133.6	126.6	127.0	125.1	125.6	125.2	124.4	122.0
Co(2)–O(4)H–Co(2)												
Co(2)–O(2)–Co(2)												
Co(2)–O(2)–X–O(3)–Co(2)	128.6	125.1	128.6	125.2	124.4	122.0	112.0	116.6	117.4	119.0	115.4	116.0

The values obtained came from the refinements from neutron diffraction patterns (D2B) at room temperature. The data for D1B at 100 K have been omitted.

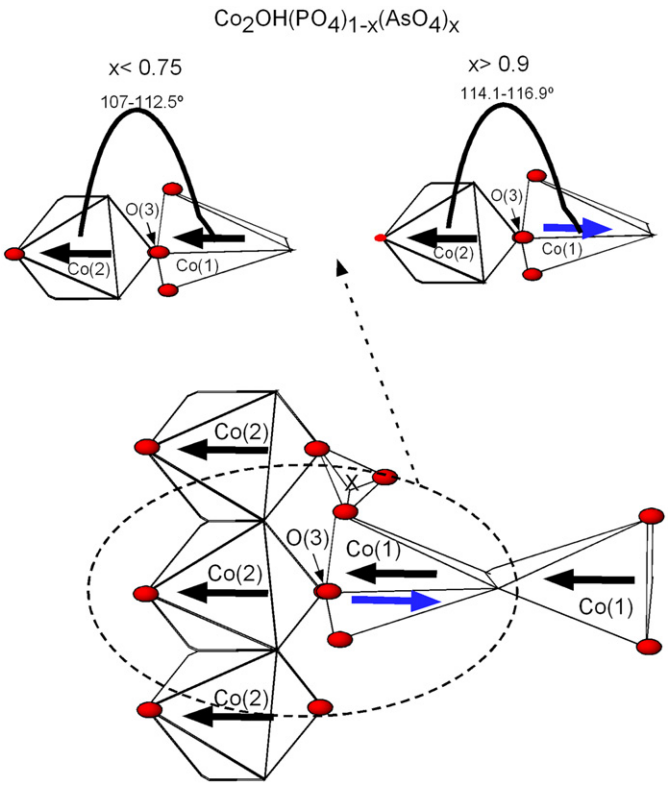

Fig. 9. Schematic view of superexchange interaction Co(1)–O(3)–Co(2) for $Co_2(OH)(PO_4)_{1-x}(AsO_4)_x$ $[0 \le x \le 1]$.

vector, k, to (0, 0.43, 0) leading to an incommensurate phase with antiferromagnetic interactions (sinusoidally amplitude modulated) (Figs. 6 and 9). Thus, this superexchange interaction, which changes with anion substitution, can be considered as crucial for the stability of the collinear AF structure, with the crossover at around 114°. Finally, the magnetic interactions via $|XO_4|$ tetrahedra (X=P, As), characterized by both the O–X–O, X–O–Co angles, induce a antiferromagnetic three-dimensional ordering.

4. Conclusions

The magnetic properties of the isomorphous compounds, $Co_2(OH)(PO_4)_{1-x}(AsO_4)_x$ $[0 \le x \le 1]$, are strongly influenced by the anion size. All phases show the existence of predominant antiferromagnetic interactions, exhibiting at lower temperatures a three-dimensional magnetic ordering. The Neel temperature decreases as the amount of arsenate ions increases. The $Co_2(OH)(PO_4)_{1-x}(AsO_4)_x$ $[0.1 \le x \le 0.75]$ phases show collinear commensurate antiferromagnetic structures. The obtained magnetic moment per Co^{2+} ion at 2 K decreases with anion substitution. This behaviour is associated with the strong anisotropy of the Co^{+2} ions and the increasing of bond-frustration of the magnetic sites [Co(2) octahedral chains and Co(1) trigonal bipyramidal dimmers]. On the other hand, the $Co_2(OH)(PO_4)_{0.1}(AsO_4)_{0.9}$ and Co_2OHAsO_4 compounds exhibit an incommensurate AF, with a strong increase in the magnetic moment in both sublattices. The explanation of this evolution must be based on the change of the superexchange magnetic pathways, as obtained with high resolution powder neutron diffraction. Of all these angles, the one observed in the frustrated magnetic pathway Co(1)–O(3)–Co(2), increases from 107° for x=0 to 112.5° for x=0.75, keeping the ferromagnetic coupling and therefore enhancing the degree of bond-frustration in the collinear AF structure. For higher anion substitution ($x \ge 0.9$), the value of this superexchange angle rises to 114.1° and 116.9° for x=0.9 and 1, respectively, inducing changes in the magnetic coupling (from F to AF) that lead to a magnetic ordering modulated in amplitude.

Acknowledgments

This work was financially supported by Basque Country Government Grant IT-312-07 and by MEC research projects (MAT2008-06542-C04, MAT2011-27573-C04 and MAT 2010-19442), which we gratefully acknowledge.

Appendix A. Supplementary material

Supplementary data associated with this article can be found in the online version at doi:10.1016/j.jssc.2012.01.048.

References

[1] S.B. Wiggin, R.W. Hughes, D.J. Price, M.T. Weller, Dalton Trans. (2007) 2935–2941.
[2] N. Marx, L. Croguennec, D. Carlier, L. Bourgeois, P. Kubiak, F. Le Cras, C. Delmas, Chem. Mater. 22 (5) (2010) 1854–1861.
[3] T. Berrocal, J.L. Mesa, J.L. Pizarro, B. Bazán, M. Iglesias, A. Aguado, M.I. Arriortua, T. Rojo, Chem. Commun. (2008) 4738–4740.
[4] G. Centi, F. Trifiro, J.R. Ebner, V.M. Franchetti, Chem. Rev. 88 (1988) 55–80.
[5] R.C. Haushalter, L.A. Mundi, Chem. Mater. 4 (1992) 31–48.
[6] Q. Chen, R.C. Haushalter, J. Zubieta, C.J. O'Connor, Science 259 (1993) 1596–1599.
[7] A. Clearfield, Chem. Rev. 88 (1998) 125–148.
[8] A. Belik, M. Azuma, A. Matsuo, M.H. Whangbo, H.J. Koo, Inorg. Chem. 44 (2005) 6632–6640.
[9] F. Xiao, J. Sun, X. Meng, R. Yu, J. Catal. 199 (2001) 273–281.
[10] F. Xiao, J. Sun, X. Meng, R. Yu, H. Yuan, D. Jiang, S. Qiu, R. Xu, Appl. Catal., A 207 (2001) 267–271.
[11] X. Meng, K. Lin, J. Sun, R. Yu, D. Jiang, F. Xiao, Catal. Lett. 71 (2001) 241–244.
[12] F.C. Hawthrone, Can. Mineral. 14 (1976) 143–148.
[13] P.B. Moore, J.R. Smyth, Am. Mineral. 53 (1968) 1841–1845.
[14] A. Cordsen, Am. Mineral. 16 (1978) 153–157.
[15] R.S.W. Braithwaite, R.G. Prichard, W.H. Paar, R.A.D. Pattrick, Mineral. Mag. 69 (2) (2005) 145–153.
[16] U. Kolitsch, Acta Crystallogr., Sect. E 59 (9) (2003) 125–128.
[17] (a) K.I. Taasti, A.N. Christensen, P. Norby, J.C. Hanson, B. Lebech, H.J. Jakobsen, J. Skibsted, J. Solid State Chem. 164 (2002) 42–50;
(b) A. Dal Negro, G. Guiseppetti, J.M.Martin Pozas, Tscherm Mineral. Petrol. Mitt. 21 (1974) 246–260.
[18] G. Raade, M.H. Mladeck, Lithos 12 (1979) 283–287.
[19] G. Raade, C. Rømming, Z. Kristallogr. 177 (1986) 1–13.
[20] A.G. Nord, P. Kierkegaard, T. Stefanidis, J. Baran, Chem. Commun. 5 (1988) 841–848.
[21] H. Strunz, E.H. Nickel, Strunz Mineralogical Tables, E. Scheweizebart'sche Verlagsbuchhandlung, Stuttgart, 2001.
[22] J.M. Rojo, J.L. Mesa, L. Lezama, J.L. Pizarro, M.I. Arriortua, J. Rodriguez Fernandez, G.E. Barberis, T. Rojo, Phys. Rev. B 66 (2002). 094406/1-094406/13.
[23] I. de Pedro, V. Jubera, J.M. Rojo, L. Lezama, J. Sanchez Marcos, J. Rodrıguez Fernandez, J.L. Mesa, T. Rojo, M.I. Arriortua, J. Magn. Magn. Mater. 272–276 (2004) e665–666.
[24] I. de Pedro, J.M. Rojo, M. Insausti, J.L. Mesa, M.I. Arriortua, T. Rojo, Z. Anorg. Allg. Chem. 631 (2005) 2096–2100.
[25] I. de Pedro, J.M. Rojo, V. Jubera, J. Rodríguez-Fernández, J. Sánchez-Marcos, L. Lezama, T. Rojo, J. Mater. Chem. 14 (2004) 1157–1163.
[26] I. de Pedro, J.M. Rojo, J.L. Pizarro, J. Rodríguez Fernández, J. Sánchez Marcos, M.T. Fernández-Diaz, M.I. Arriortua, T. Rojo, J. Phys. Condens. Matter 18 (2006) 3767–3787.
[27] I. de Pedro, J.M. Rojo, J.L. Pizarro, J. Rodríguez Fernández, J. Sánchez Marcos, M.T. Fernández-Diaz, M.I. Arriortua, T. Rojo, J. Mater. Chem. 17 (2007) 3915–3926.
[28] (a) I. de Pedro, J.M. Rojo, L. Lezama, T. Rojo, Z. Anorg. Allg. Chem. 633 (2007) 1847–1852;
(b) I. de Pedro, J.M. Rojo, J.L. Pizarro, J. Rodríguez Fernández, M.I. Arriortua, T. Rojo, J. Solid State Chem. 184 (2011) 2075–2082.
[29] I. de Pedro, J.M. Rojo, J. Rodríguez Fernández, M.T. Fernández-Díaz, T. Rojo, Phys. Rev. B 81 (2010). 134431/1-134431/14.
[30] I. de Pedro, J.M. Rojo, J. Rodríguez Fernández, L. Lezama, T. Rojo, Eur. J. Inorg. Chem. (2010) 2514–2522.

[31] B.F. Alfonso, C. Trobajo, C. Pique, M.T. Fernández-Díaz, J. Rodríguez Fernández, M.A. Salvado, P. Pertierra, S. García-Granda, J.R. García, J.A. Blanco, Acta Mater. 58 (2010) 1741–1749.
[32] M. Kurmoo, Chem. Soc. Rev. 38 (5) (2009) 1353–1379.
[33] J.A. Mydosh, Spin Glasses: An Experimental Introduction, Taylor & Francis, London, 1993.
[34] K. Moorjani, J.M.D. Coey, Magnetic Glasses, in: S.P. Wolsky, A.W. Czanderna (Eds.), Methods and Phenomena, Vol. 6, Elsevier, Amsterdam, 1984.
[35] J. Rodríguez-Carvajal, FULLPROF program for rietveld refinement and pattern matching analysis of powder patterns, Phys. B 192 (1993) 55. and unpublished later versions. The program is a strongly modified version of that described by D.B. Wiles, R.A. Young, J. Appl. Crystallogr. 14 (1981) 149.
[36] W.T.A. Harrison, J.T. Vaughey, L.L. Dussack, A.J. Jacobson, T.E. Martin, G.D. Stucky, J. Solid State Chem. 114 (1995) 151–158.
[37] P. Séller, H. Hess, F. Zettler, Neues Jahrb. Mineral. Abh. 334 (1979) 27–34.
[38] H.M. Rietveld, J. Appl. Crystallogr. 2 (1969) 65–71.
[39] A.T. Petit, P.L. Dulong, Ann. Chim. Phys. 10 (1819) 395.
[40] P. Debye, Ann. Phys. 344 (1912) 789.
[41] P. Sengupta, A.W. Sandvik, R.R.P. Singh, Phys. Rev. B 68 (2003)094423/1-094423/7 68 (2003).
[42] Y.A. Izymov, V.E. Naish, R.P. Ozerov, Neutron Diffraction of Magnetic Materials, Consultants Bureau, New York, 1991.
[43] J. Rodríguez-Carvajal, BASIREPS, 〈ftp://ftp.cea.fr/pub/llb/divers/BasIreps〉.
[44] M.E. Foglio, M.C. dos Santos, G.E. Barberis, J.M. Rojo, J.L. Mesa, L. Lezama, T. Rojo, J. Phys.: Condens. Matter. 14 (2002) 2025–2041.
[45] (a) M.G. Barandika, Z. Serna, R. Cortes, L. Lezama, M.K. Urtiaga, M.I. Arriortua, T. Rojo, Chem. Commun. (2001) 45–49;
(b) Z. Serna, M.K. Urtiaga, M.G. Barandika, R. Cortes, L. Lezama, M.I. Arriortua, T. Rojo, Inorg. Chem. 40 (2001) 4550–4555.
[46] J.B. Goodenough, Magnetism and the Chemical Bond, Interscience, New York, 1963.
[47] O. Khan, Inorg. Chem. 3 (1984) 105–132.
[48] O. Khan, Struct. Bond. (Berlin) 68 (1987) 89–176.